Two Regimes of Turbulent Fluxes Above a Frozen Small Lake Surrounded by Forest

Kirill Barskov[1,2] (ID) · **Victor Stepanenko[2,3]** · **Irina Repina[1,2]** · **Arseniy Artamonov[1]** · **Alexander Gavrikov[4]**

Abstract

We present experimental results of turbulent heat exchange between a small frozen lake surrounded by forest and the atmospheric boundary layer. Heat fluxes are measured at three levels using the eddy-covariance method and estimated by Monin–Obukhov similarity theory (MOST). In addition, we estimate the heat flux due to non-local turbulent transport of heat by coherent structures originating at the forest/lake transition, given the measured skewness of w' and $\overline{w'w'T'}$, using a bimodal bottom-up–top-down model or the mass-flux models appropriate to the convective boundary layer. Two heat-flux-formation regimes in the surface layer are clearly distinguished. When the flow is from the vast forest, wind shear at the tree height leads to increased turbulent kinetic energy above the centre of the lake. Under conditions of simultaneous horizontal advection of warm air in the boundary layer above the canopy, a downward turbulent diffusion of negative heat flux leads to increased negative sensible heat flux in the surface layer, accompanied by an increasing third moment $\overline{w'w'T'}$. Since MOST does not account for this mechanism, MOST-based fluxes poorly correspond to the eddy-covariance data in this case. At the same time the contribution of coherent structures increases. In contrast, when the flow is from the gap connecting the lake with the wide clearing, the effects of landscape inhomogeneity significantly reduce. In this case the turbulent transport of the heat flux from the upper part of the boundary layer vanishes, $\overline{w'w'T'}$ is negligible, and the heat flux is now primarily determined by the wind speed and temperature differences between the surface and near-surface atmosphere. This is a surface-flow regime for which MOST has been developed, and MOST-based fluxes correlate well with eddy-covariance data.

Keywords Eddy covariance · Forest lake · Inhomogeneous surface · Monin–Obukhov similarity theory · Turbulence

✉ Kirill Barskov
  barskov@ifaran.ru

1 A.M. Obukhov Institute of Atmospheric Physics, RAS, Moscow, Russia 119017

2 Research Computing Center, Moscow State University, Moscow, Russia 119234

3 Faculty of Geography, Moscow State University, Moscow, Russia 119234

4 P.P.Shirshov Institute of Oceanology, RAS, Moscow, Russia 117997

1 Introduction

In lake-rich continental regions, especially in northern Europe and Canada, small lakes exert a large influence on the balance of heat and moisture in the boundary layer (Rouse et al. 2005). As found previously (Balsamo et al. 2012; Martynov et al. 2012; Subin et al. 2012), taking lakes into account in climate and weather prediction models produces significant local and global response in the atmospheric circulation.

For the past several decades the Monin–Obukhov similarity theory (MOST) has been widely used to parametrize energy and mass exchange between the surface and the atmosphere. It assumes a homogeneous horizontal distribution of the surface characteristics and of the flow properties, and therefore provides high-accuracy prediction of the fluxes for homogeneous landscapes (Mordukhovich and Tsvang 1966; Koprov and Sokolov 1975; Stull 1988; Sorbjan 1989; Garratt 1994; Kaimal and Finnigan 1994; Wyngaard 2010). Many lakes in Northern Russia and Europe are surrounded by forests, conditions that cannot be considered homogeneous, and using MOST to compute heat exchange in the surface layer may lead to significant errors. The structure of the turbulent flow near the downwind forest edge may resemble the structure of a backwardfacing step flow with the formation of a recirculation zone with a quasi two-dimensional vortex in the vertical plane (Condie and Webster 2001; Boehrer and Schultze 2008; Markfort et al. 2010; Kenny et al. 2017). Large-eddy simulation (LES) results show that close to the shore (at a distance of less than 15–20 tree heights), the fluxes based on eddy correlation (eddy-covariance fluxes) at typical levels of measurements (2 m) significantly differ from the surface fluxes, probably due to the intense production of TKE (E) and second turbulent moments (fluxes) induced by the large velocity shear at tree height (Glazunov and Stepanenko 2015; Kenny et al. 2017). It was also shown that flux observations in the coastal regions require at least a two-tower system to account for the effect of horizontal advection (Camilo et al. 2017). Thus, widespread single-level eddy-covariance measurements may mislead the determination of energy and mass exchange between small lakes and the atmosphere.

Here we investigate the heat and momentum exchange between a forest lake and the atmosphere in winter using three levels of eddy-covariance measurements. Particularly, we examine the applicability of MOST for estimating the heat exchange at the lake–atmosphere interface. The data collected during the observational campaign described below were first analyzed in Barskov et al. (2017). It was shown that the eddy-covariance fluxes agreed well with those obtained using the surface-energy-balance method, but MOST failed to reproduce the sharp increase in the negative heat flux at the surface layer for some time intervals, and agreed well with the eddy-covariance fluxes for the other time intervals. Here we analyze the third-order moments and the conditions of applicability of MOST for calculating the sensible heat flux.

2 Site and Measurements

The measurements were conducted from 25 January 2017 to 3 February 2017 on Kislo-Sladkoe Lake in the neighbourhood of the White Sea Biological Station (WSBS) operated by Moscow State University. The location of the lake centre is 66°32′52.5186″N, 33°08′8.865″E (Grum-Grzhimaylo et al. 2016). Sunrise took place at about 1030 LT (local time is UTC + 3 h) and sunset at about 1550 LT, whole frozen lake dimensions are approximately 200 m by 150 m. The southern and western sides of the lake are bordered by vast forest landscapes (Fig. 3a),

and northern and eastern sides are bordered by a forest belt (50–100 m width) separating the lake from the gulf. There are two 30-m wide gaps in the forested areas that serve as open surfaces "connecting" the lake with the gulf. More detailed climatic and geomorphological characteristics of this area have been given in Grum-Grzhimaylo et al. (2016, 2018).

The 6-m mast was installed in the centre of the lake. Temperature fluctuations and three wind-speed components were measured using a WindMaster HS 3D anemometer (Gill Instruments, UK) at 2-m level and WindMaster 3D anemometer (Gill Instruments, UK) at 4 m and 6 m with a 20-Hz frequency. Humidity and temperature measurements were made at automatic meteorological stations Davis Vantage Pro 2 (Davis Instruments, USA), at 3 m and 5 m. A soil station (Davis Instruments, USA) was deployed at the distance of about 10 m from the mast to measure the temperature of the snow cover at four depth levels including the surface. Measurements on the lake included the temperature profile in the atmospheric boundary layer from the surface up to 1 km with 50-m step, made using a microwave profiler MTP-5 (Attex, Russian Federation).

With this set-up, we obtain the sensible heat flux H at levels 2 m, 4 m, and 6 m using the eddy-covariance method. Alternatively, we calculated H using the MOST-based gradient method with temperature measurements at 3 m and 5 m and wind speed at 2 m, 4 m, and 6 m. Thus, we avoided specifying the roughness length.

3 Data Processing

The eddy-covariance fluxes were based on 30-min averaging using the EddyUH software package (Mammarella et al. 2016). Data preprocessing included despiking, 2D coordinate rotation for the velocity components, linear detrending, and time lag determination. Several corrections were also applied to the 30-min covariance: spectral correction, density correction (Webb et al. 1980), and humidity correction of the sonic temperature. More details on data processing are given in Barskov et al. (2017).

The gradient method assumes that all statistical characteristics of the temperature, humidity, and velocity fields normalized to the corresponding scales for temperature T_*, humidity q_*, and velocity u_* are described by universal functions of the dimensionless height $\xi = z/L$, where L is the Obukhov length and z is the height of measurements. Universal functions used here are described in the Appendix. All methods assume positive fluxes to be directed upward.

4 Heat-Flux Balance Equation and Third Moments

For diagnosing the mechanisms governing the turbulent heat flux in the surface layer, a flux balance equation is used

$$\underbrace{\frac{\partial \overline{w'T'}}{\partial t}}_{I} = -\underbrace{\overline{w'u'_k}\frac{\partial \bar{T}}{\partial x_k}}_{II} - \underbrace{\overline{u_k}\frac{\partial \overline{T'w'}}{\partial x_k}}_{III} - \underbrace{\overline{T'u'_k}\frac{\partial \bar{w}}{\partial x_k}}_{IV} - \underbrace{\frac{\partial \overline{u'_k w'T'}}{\partial x_k}}_{V}$$

$$+ \underbrace{\overline{w'\kappa\nabla^2 T'} + \overline{T'\vartheta\nabla^2 w}}_{VI} - \underbrace{\frac{1}{\rho_0}\overline{T'\frac{\partial p'}{\partial z}}}_{VII} + \underbrace{\frac{g}{T_0}\overline{T'^2}}_{VIII},$$

$$(1)$$

where Einstein summation notation is assumed. Equation 1 is more exact being expressed in terms of potential temperature, but hereafter we assume $\Theta' \approx T'$ as an acceptable approximation for the surface layer. The left-hand side (l.h.s) is the heat-flux tendency (I), and right-hand side (r.h.s.) terms are, in order, production by the temperature gradient (II), the temperature-flux advection (III), the vertical wind-shear production (IV), the third-moment turbulent transport (V), dissipation (VI), the pressure production (VII), and the buoyancy generation (VIII). Below we only consider the third-moment turbulent transport of the heat flux in the boundary layer expressed by term V. The assumption $\overline{w'w'T'}\big|_{z=0} = 0$ may be used to approximate the vertical derivative in term V in the surface layer as $\frac{\partial \overline{w'w'T'}}{\partial z} \approx \frac{\overline{w'w'T'}}{z}$. Thus, a rise in $\overline{w'w'T'}$ at the measurement level indicates an increase in the turbulent transport contribution to the heat-flux tendency.

Large-eddy simulation of airflow developing over a small round or elliptical inland lake surrounded by a forest shows that there are lake-scale and canopy-scale secondary circulations emerging (Glazunov and Stepanenko 2015). One result of the secondary circulations is the formation of persistent vertical updrafts and downdrafts near the forest–lake transitions that drive complex persistent patterns of the horizontal and vertical advection of scalars (Kenny et al. 2017). Because of the inhomogeneity of the landscape around the Kislo-Sladkoe Lake and the complexity of the forest structure around, spatial distribution of areas affected by the large eddies formed at the edge depends on the wind direction. That is why one could expect varied skewness of probability distributions at the point of measurement in different regimes of external forcing. The presence of large coherent structures with updrafts and downdrafts that are likely to have significant contributions to the vertical fluxes suggests using statistical methods for flux estimation developed for the convective boundary layer. Specifically, the vertical turbulent advection of the heat flux in a bimodal bottom-up–top-down model (Zilitinkevich et al. 1999) or in a mass-flux model (Abdella and McFarlane 1997) is proportional to the heat flux, with the proportionality coefficient including the skewness of vertical velocity S_w

$$\overline{w'w'T'} = C_T S_w \left(\overline{w'^2}\right)^{1/2} \overline{w'T'}, \tag{2}$$

where C_T is a dimensionless constant. This result may be applied to eddy-covariance measurements as well, if the averaging operator is treated as temporal averaging. Substituting probabilistic averaging (Zilitinkevich et al. 1999) or spatial averaging (Abdella and McFarlane 1997) by temporal averaging means that, along with a possible quasi-stationary rotor at the forest margin, we assume coherent structures advected by the horizontal airflow from the forest edge towards the measurement point.

It has been shown for the convective boundary layer that the third-order moment is largely responsible for the non-local nature of turbulent transport (Zilitinkevich et al. 1999). Likewise, in our case, the magnitude of the third moment $\overline{w'w'T'}$ may indicate non-local turbulent transport of the heat flux by coherent structures originating at the forest–lake transition. To check this hypothesis, one may compare the eddy-covariance heat flux (H_{EC}) to the heat flux due to coherent structures (H_{CS}), computed from Eq. 2, given the measured skewness of w' and $\overline{w'w'T'}$, as

$$H_{CS} = -C_p \rho \overline{w'T'} = -C_P \rho \frac{\overline{w'w'T'}}{S_w \left(w'^2\right)^{\frac{1}{2}}}, \tag{3}$$

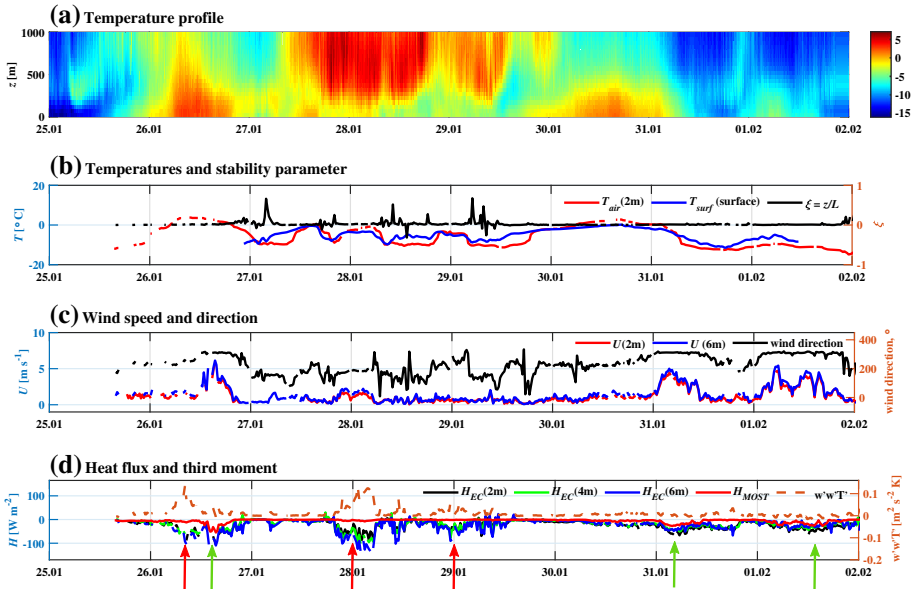where C_p is the heat capacity of air and ρ is air density.

Fig. 1 The temperature profile up to 1 km (**a**), air temperature at 2 m, temperature at the surface and stability parameter ξ (**b**), wind speed and direction (**c**), and time series of sensible heat flux, measured directly (H_{EC}) at 2, 4, and 6 m, calculated by MOST H_{MOST}, and third moment $\overline{w'w'T'}$ (**d**). Dates are from 25 January to 2 February

5 Results and Discussion

5.1 Two Regimes of Turbulent Fluxes

Figure 1 shows the temperatures at the surface and at 2-m height, the stability parameter $\xi = z/L$, vertical temperature profile up to 1 km, time series of sensible heat flux calculated by the gradient method (H_{MOST}), turbulent heat flux measured at 2, 4, and 6 m (H_{EC}) and the third moment $\overline{w'w'T'}$ at a height of 6 m.

Most of the time, surface-layer stratification does not deviate much from near-neutral ($|\xi| < 0.05$) and sometimes is weakly stable ($0.1 < \xi < 0.5$), Fig. 1b. One can see time intervals (e.g. around 0000, 28 January) when the magnitude of H_{EC} significantly increases with height, violating the constancy of flux with height, one of the key assumptions underlying MOST.

Two scenarios are notable in the temporal characteristics of the heat flux. The first scenario is denoted by green arrows (Fig. 1d), for which the gradient method agrees well with the direct measurements, albeit being smaller in absolute value. Wind direction in these cases is from 295° to 325° (the flow is from the gap, so the flow freely enters the interior of the forest-bounded lake) and the near-surface wind speed for these intervals is about 5–6 m s^{-1}. The heat-flux transport from above ($\overline{w'w'T'}$) is relatively small, so that heat and momentum fluxes are formed primarily due to interaction of the turbulent flow with the local surface—the scenario assumed in MOST.

The second scenario is denoted by the red arrows when there is a significant increase in the eddy-covariance fluxes while MOST-calculated fluxes almost vanish. Note that the wind
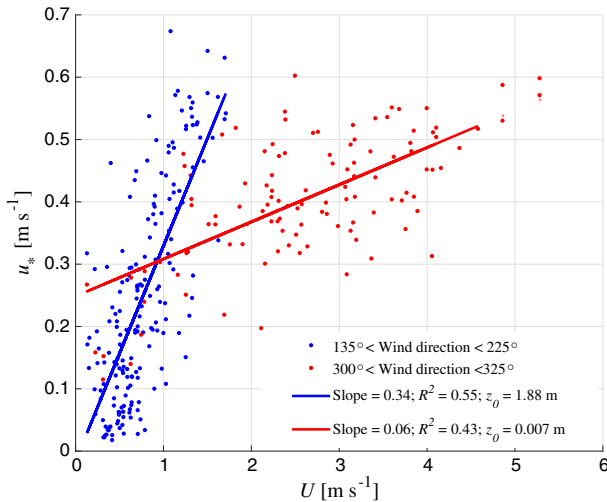
Fig. 2 Dependence of u_* on wind speed under different wind direction

direction in such cases is from 135° to 225° (the airflow is from the vast forest) and the wind speed remains small (<2 m s^{-1}), so MOST does not provide an increase in heat flux. Due to the small wind speed, one may also expect a minor role of mean-wind related terms III and IV in Eq. 1. At these times, the heat flux is much more sensitive to the wind speed than that calculated by MOST: an increase from 1 to 2 m s^{-1} causes an increase in the third moment $\overline{w'w'T'}$ in the surface layer and absolute values of the heat flux increase from 40 to 120 W m^{-2}. At the same time MOST-calculated fluxes increase only from 1 to 8 W m^{-2}. This corresponds well with conclusions in Grachev et al. (2018), viz. that flux-profile relationships are severely violated downwind of sharp roughness discontinuities. Small increases of the wind speed significantly increases u_* in the surface layer in this scenario (Fig. 2).

Based on MOST, at a given observation height z, the slope of u_* versus U is proportional to $1/\ln(z/z_0)$, where z_0 is the aerodynamic roughness length. One can see that there is a very sharp change in the effective roughness length between the cases when the flow is from the gap or from the forest (slope changes from 0.06 to 0.34 and calculated z_0 changes from 0.007 to 1.8 m). We suppose the reason is that most of the turbulent kinetic energy in the case of flow through the forest is produced by wind shear at the tree height and then transported downwards (Glazunov and Stepanenko 2015). These periods coincide with warm-air advection in the middle and upper part of the boundary layer (Fig. 1a). At the same time $\overline{w'w'T'}$ increases in the surface layer (Fig. 1d). One can expect that large turbulent kinetic energy at and above tree height combined with the vertical temperature gradient from tree height to approximately 100 m (see $\overline{w'^2}d\bar{T}/dz \sim Ed\bar{T}/dz$ as part of term II of Eq. 1) increase the heat flux, which is then transported downwards to the surface layer, contributing to the large observed near-surface H_{EC}. However, the mean temperature profile measurements above the landscape available in our case alone do not allow for a robust verification of this hypothesis.

5.2 Applicability of the MOST for Sensible Heat Flux

Firstly, we estimated the errors of the gradient method caused only by measurement errors. Accuracy of the wind-speed measurement is $\varepsilon_{usa} = \Delta U_{USA}/U = 1.5\%$, typical wind speeds

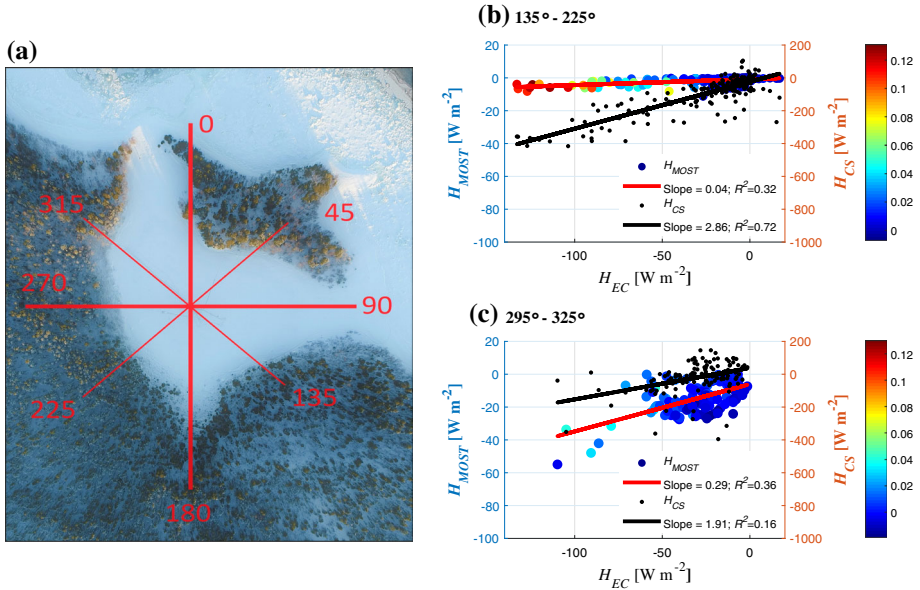**Fig. 3** Lake with wind-directions diagram (**a**), scatter plot H_{MOST} and H_{CS} versus H_{EC} when the flow is from the vast forest (**b**), and from the northern gap (**c**). Colour scale is given for the third moment $\overline{w'w'T'}$

in our measurements were 2–5 m s^{-1} and a typical difference between wind speed at 2 and 6 m was 0.3–0.6 m s^{-1}. The error of temperature measurements is $\Delta T_{davis} = 0.3$ K, and the typical difference between temperature values at 3 m and 5 m was 0.3–0.5 K. Due to the independence between wind-speed and temperature measurements, we can estimate the relative error

$$\in_{MOST} = \frac{\Delta H_{MOST}}{H_{MOST}} = \sqrt{\left(\frac{\Delta (U_*)}{(U_*)}\right)^2 + \left(\frac{\Delta (T_*)}{(T_*)}\right)^2}$$

$$\sim \sqrt{\left(\frac{\Delta (U_2 - U_1)}{(U_2 - U_1)}\right)^2 + \left(\frac{\Delta (T_2 - T_1)}{(T_2 - T_1)}\right)^2} = \sqrt{\left(\frac{2\Delta U_{USA}}{(U_2 - U_1)}\right)^2 + \left(\frac{2\Delta T_{davis}}{(T_2 - T_1)}\right)^2}. \tag{4}$$

Calculated ε_{MOST} is from 100 to 300% throughout the experiment, so a precise match between the MOST and eddy-covariance measurements is unlikely, but we can distinguish periods when two methods, (1) provide correlating results, and (2) differ by several orders of magnitude.

According to the two regimes of turbulent fluxes described in Sect. 5.1, we suppose that the measured heat flux H_{EC} may be formed by non-local advection of the coherent structures (H_{CS}) or by near-surface wind speed and temperature gradients (H_{MOST}), with a scatter plot H_{EC} versus H_{MOST} and H_{CS} in the two cases given at Fig. 3.

When the flow is through the vast forest (Fig. 3b) the slope for H_{MOST} versus H_{EC} is 0.04, so MOST is not applicable. Increases in the H_{EC} magnitude is accompanied by increases in $\overline{w'w'T'}$ (colour of dots) and H_{CS} significantly increases (black dots) with a slope 2.86. The slope is not expected to be equal to 1, because Eq. 2 is derived using the mass-flux approximation only, while in a more general case, the dimensionless constant C_T may not be equal to 1. There is a good correlation between H_{CS} and H_{EC} in this case, $R^2 = 0.7$.

When the flow is through the northern gap (Fig. 3c) the scatter slope for H_{MOST} versus H_{EC} is seven times larger (0.29 instead of 0.04) and the third moment $\overline{w'w'T'}$ is close to zero (colour of the dots). This implies that MOST reproduces eddy-covariance fluxes though underestimating the absolute values when the flow is from the northern gap. At the same time, H_{CS} has positive or close to zero values (up to $|H_{EC}| < 50$), while the measured flux is negative. Only large values of H_{EC} are accompanied by increases in $\overline{w'w'T'}$ and H_{CS}, but less than those in the first case: $\overline{w'w'T'} = 0.04$ instead of 0.1 and the general scatter slope H_{CS} versus H_{EC} is 1.5 times smaller (1.91 instead of 2.86), and the coefficient of determination $R^2 = 0.16$ in this case, i.e. Eq. 2 is not valid and the contribution of coherent structures is negligible.

As shown by Barskov et al. (2017), the surface-layer eddy-covariance sensible and latent heat fluxes measured in this field experiment correlate well with fluxes estimated from the snow and ice heat balance. Thus, the heat exchange between the winter lake surrounded by forest and the atmosphere in the case of a cross-lake wind direction is determined by downward turbulent transport (expressed by the third moment $\overline{w'w'T'}$) of the heat flux formed in the boundary layer at and above the canopy, rather than by the near-surface wind-speed and temperature gradients.

6 Conclusion

Eddy-covariance measurements over a frozen lake surrounded by forest suggest that there are two scenarios of the turbulent heat-flux development in the surface layer. When the flow is from the vast forest, turbulence is very sensitive to the wind speed because of the wind shear at tree height. In this case, increases of the wind speed lead to significant increases of the turbulent kinetic energy at the centre of the lake. If there is advection of warm air in the boundary layer above, the turbulent diffusion $\overline{w'w'T'}$ transports negative heat flux from the flow above the trees to the surface. The MOST approach does not include this mechanism and fails to agree with the eddy-covariance heat-flux measurements. At the same time, the relation of the heat flux to $\overline{w'w'T'}$ and the skewness of vertical velocity developed for coherent structures (Abdella and McFarlane 1997; Zilitinkevich et al. 1999) correlates well with the eddy-covariance flux in this case, indicating the presence of such structures. The link of MOST performance to turbulence anisotropy (Stiperski and Calaf 2018) opens a perspective for future joint analysis of fluxes, higher-order moments, probabilistic distributions, and anisotropy parameters for turbulent flows in heterogeneous landscapes.

When the flow is from the gap connecting the lake with the homogeneous surface, the surface sensible heat flux is not closely connected to processes in the upper levels of the boundary layer and is rather determined by the near-surface wind speed and temperature difference between the surface and near-surface air. Hence, $\overline{w'w'T'}$ becomes negligible and the MOST-based calculations correlate well with the eddy-covariance method.

Appendix: General Description of MOST

The gradient method assumes that all statistical characteristics of the temperature, humidity, and wind velocity fields are normalized to the corresponding scales of the temperature T_*, humidity q_*, and velocity u_*, and are described by universal functions of the dimensionless height $\xi = z/L$, where L is the Obukhov length and z is the height. Specifically, according to the Monin–Obukhov similarity theory (MOST) the deficits of averaged meteorological variables in the surface layer obey the following relations,

$$U(z_2) - U(z_1) = \frac{u_*}{\kappa}\left(\ln\left(\frac{z_2}{z_1}\right) - \Psi_M\left(\frac{z_2}{L}\right) + \Psi_M\left(\frac{z_1}{L}\right)\right) \tag{5}$$

$$T(z_2) - T(z_1) = \frac{T_*}{\kappa}\left(\ln\left(\frac{z_2}{z_1}\right) - \Psi_H\left(\frac{z_2}{L}\right) + \Psi_H\left(\frac{z_1}{L}\right)\right) \tag{6}$$

$$q(z_2) - q(z_1) = \frac{q_*}{\kappa}\left(\ln\left(\frac{z_2}{z_1}\right) - \Psi_q\left(\frac{z_2}{L}\right) + \Psi_q\left(\frac{z_1}{L}\right)\right) \tag{7}$$

where κ is the von Kármán constant, lower indices "2" and "1" denote the two levels of measurements, $\psi_i(\xi)$, $i = M, H$, and q are dimensionless universal functions. We used the universal functions (Beljaars and Holtslag 1991) for stable stratification

$$-\Psi_M(\xi) = -\Psi_H(\xi) = -\Psi_q(\xi) = a\xi + b\left(\xi - \frac{c}{d}\right)\exp(-d\xi) + \frac{bc}{d}, \tag{8}$$

where a = 0.7, b = 0.75, c = 5, d = 0.35. The Businger–Dyer form (Businger et al. 1971; Dyer 1974) is used for unstable stratification,

$$\Psi_M(\xi) = 2\ln\left[\frac{1+x}{2}\right] + \ln\left[\frac{1+x^2}{2}\right] - 2\operatorname{arctg}(x) + \frac{\pi}{2}, \tag{9}$$

$$\Psi_{H,q}(\xi) = 2\ln\left[\frac{1+y^2}{2}\right], \tag{10}$$

where $x = (1 - 16\xi)^{1/4}$, $y = (1 - 16\xi)^{1/2}$. The turbulent fluxes are calculated from

$$\tau = \rho_0 u_*^2, \tag{11}$$

$$H = -C_p \rho_0 u_* T_* \tag{12}$$

$$L_s E = -\rho_0 L_s u_* q_*. \tag{13}$$

References

Abdella K, McFarlane N (1997) A new second-order turbulence closure scheme for the planetary boundary layer. J Atmos Sci 54:1850–1867

Balsamo G, Salgado R, Dutra E et al (2012) On the contribution of lakes in predicting near-surface temperature in a global weather forecasting model. Tellus A 64:15829

Barskov KV, Chernyshev RV, Stepanenko VM, Repina IA, Artamonov AY, Guseva SP, Gavrikov AV (2017) Experimental study of heat and momentum exchange between a forest lake and the atmosphere in winter. IOP Conf Ser Earth Environ Sci 96:012003

Beljaars AC, Holtslag AA (1991) Flux parameterization over land surfaces for atmospheric models. J Appl Meteorol 30(3):327–341

Boehrer B, Schultze M (2008) Stratification of lakes. Rev Geophys. https://doi.org/10.1029/2006RG000210

Businger JA, Wyngaard JC, Izumi Y, Bradley EF (1971) Flux profile relationships in the atmospheric surface flow. J Atmos Sci 28(2):181–189

Camilo ARS, Bohrer G, Morin TH, Shlomo D, Mirfenderesgi G, Gildor H, Genin A (2017) Evaporation and CO_2 fluxes in a coastal reef: an eddy covariance approach. Ecosyst Health Sustain 3(10):1392830

Condie SA, Webster IT (2001) Estimating stratification in shallow water bodies from mean meteorological conditions. J Hydraul Eng ASCE 127(4):286–292

Dyer AJ (1974) A review of flux-profile relationships. Boudary-Layer Meteorol 7:363–372

Garratt JR (1994) The atmospheric boundary layer. Cambridge University Press, Cambridge

Glazunov AV, Stepanenko VM (2015) Large-eddy simulation of stratified turbulent flows over heterogeneous landscapes. IZV Atmos Ocean Phys 51(4):351–361

Grachev AA, Leo LS, Fernando HJS, Fairall CW, Creegan E, Blomquist BW, Christman AJ, Hocut CM (2018) Air–sea/land interaction in the coastal zone. Boundary-Layer Meteorol 167(2):181–210

Grum-Grzhimaylo OA, Debets AJM, Bilanenko EN (2016) The diversity of microfungi in peatlands originated from the White Sea. Mycologia 108(2):233–254

Grum-Grzhimaylo OA, Debets AJM, Bilanenko EN (2018) Mosaic structure of the fungal community in the Kislo-Sladkoe Lake that is detaching from the White Sea. Polar Biol 41(10):2075–2089

Kaimal JC, Finnigan JJ (1994) Atmospheric boundary layer flows: their structure and 860 measurements. Oxford University Press, Oxford

Kenny WT, Bohrer G, Morin TH et al (2017) A numerical case study of the implications of secondary circulations to the interpretation of eddy-covariance measurements over small lakes. Boundary-Layer Meteorol 165(2):311–332

Koprov BM, Sokolov DY (1975) About the experimental study of the variability of the heat flux in the boundary layer of the atmosphere. Bull Acad Sci USSR Phys Atmos Ocean 11(77):743–747

Mammarella I, Peltola O, Nordbo A, Järvi L, Rannik Ü (2016) Quantifying the uncertainty of eddy covariance fluxes due to the use of different software packages and combinations of processing steps in two contrasting ecosystems. Atmos Meas Tech 9:4915–4933

Markfort CD, Perez ALS, Thill JW, Jaster DA, Porté-Agel F, Stefan HG (2010) Wind sheltering of a lake by a tree canopy or bluff topography. Water Resour Res. https://doi.org/10.1029/2009WR007759

Martynov A, Sushama L, Laprise R, Winger K, Dugas B (2012) Interactive lakes in the Canadian Regional Climate Model, version 5: the role of lakes in the regional climate of North America. Tellus A 64:16226

Mordukhovich MI, Tsvang LR (1966) Direct measurements of turbulent flows at two levels in the ground layer of the atmosphere. Bull Acad Sci USSR Phys Atmos Ocean E2(8):786–803

Rouse WR, Oswald CJ, Binyamin J et al (2005) The role of northern lakes in a regional energy balance. J Hydrometeorol 6(3):291–305

Sorbjan Z (1989) Structure of the atmospheric boundary layer. Prentice-Hall, New Jersey

Stiperski I, Calaf M (2018) Dependence of near surface similarity scaling on the anisotropy of atmospheric turbulence. Q J R Meteorol Soc 144(712A):641–657. https://doi.org/10.1002/qj.3224

Stull RB (1988) An introduction to boundary-layer meteorology. Kluwer, Boston

Subin ZM, Riley WJ, Mironov D (2012) An improved lake model for climate simulations: model structure, evaluation, and sensitivity analyses in CESM1. J Adv Model Earth Syst 4(1):M02001

Webb EK, Pearman GI, Leuning R (1980) Correction of flux measurements for density effects due to heat and water vapour transfer. Q J R Meteorol Soc 106:85–100

Wyngaard JC (2010) Turbulence in the atmosphere. Cambridge University Press, New York

Zilitinkevich S, Gryanik VM, Lykossov VN, Mironov DV (1999) Third-order transport and nonlocal turbulence closures for convective boundary layers. J Atmos Sci 56:3463–3477